Classification of High Frequency Oscillations in intracranial EEG signals based on coupled time-frequency and image-related features

Fatma Krikid [1,2,3*], Ahmad Karfoul [2], Sahbi Chaibi [1], Amar Kachenoura [2], Anca Nica [4], Abdennaceur Kachouri [1,3], Régine Le Bouquin Jeannès [2]

[1] LETI-ENIS, University of Sfax, Street of Soukra, 3038 Sfax, Tunisia
[2] Univ Rennes, Inserm, LTSI - UMR 1099, F-35000 Rennes, France
[3] AFDE-ENIS, University of Sfax, Street of Soukra, 3038 Sfax, Tunisia
[4] CHU de Rennes, Service de Neurologie, Pôle des Neurosciences, Cliniques de Rennes, F-35000 Rennes, France
[*] fatma.krikid@etudiant.univ-rennes1.fr

Abstract—— High Frequency Oscillations (HFOs) occurring in the range of [30-500 Hz] in epileptic intracranial ElectroEncephaloGraphic (iEEG) signals have recently proven to be good biomarkers for localizing the epileptogenic zone. Identifying these particular cerebral events and their discrimination from other transient events like interictal epileptic spikes is traditionally performed by experts through a visual inspection. However, this is laborious, very time-consuming and subjective. In this paper, a new classification approach of HFOs is proposed. This approach mainly relies on the combination of raw time frequency (TF) features, computed from a TF representation of HFOs using S-transform, with relevant image-based ones derived from a binarization of the corresponding TF grayscale image. The obtained feature vector is then used to learn a multi-class Radial Basis Function (RBF) based Support Vector Machine (SVM) classifier. The efficiency of the proposed approach, compared to conventional classification schemes based only on time, frequency or energy-based features, is confirmed, using both simulated and real iEEG signals. The proposed classification system has achieved, using simulated data and a signal to noise ratio (SNR) of 15 dB, a sensitivity, specificity, accuracy, area under the curve and F1-score around 0.990, 0.996, 0.995, 0.993 and 0.990 respectively. Besides, for real data, our proposed approach has attained the scores of 0.765, 0.941, 0.906, 0.929 and 0.768 for sensitivity, specificity, accuracy, area under the curve and F1-score respectively. These results confirm the relevance of coupling TF and image-related features, in the way proposed in this paper, for higher HFOs classification quality compared to already existing approaches.

Keywords— Epilepsy; High Frequency Oscillations; Time frequency representation; Image gradient; Sparsity; Multi-classification; SVM.

I. INTRODUCTION

Around 65 million people worldwide are affected by epilepsy which can be characterized by recurrent seizures [1]. However, more than 30% of patients are drug resistant and a surgical resection of the Epileptogenic Zone (EZ) stands for the best therapeutic solution to reduce the occurrence of such seizures [2]. The success of resection surgery mainly depends on the localization of the EZ. The epilepsy can be diagnosed through different neuroimaging modalities (functional and structural) [3]. In this context, recent studies have proposed various algorithms [4], [5] to diagnose epileptic seizures. More recently, High Frequency Oscillations (HFOs) have gained particular attention as promising biomarkers of the EZ [2], [6]. HFOs, occurring in epileptic human intracranial ElectroEncephaloGraphic (iEEG) signals, are non-stationary oscillations with consecutive oscillations in the frequency band [30-500 Hz] that can be distinguished from the baseline [6]. Frequently, researchers divide the HFOs into two bands, namely Ripples (Rs, [80-250 Hz]) and Fast Ripples (FRs, [250-500 Hz]) [2], [6]. Actually, in some studies, authors have proven that HFOs bands also include Gamma (γ, [30-80 Hz])

Accepted manuscript / Final version

Table 1. An overview on HFOs classification methods.

Study	Features	Classification techniques	Context
Firpi et al. 2007 [16]	Particle swarm optimization	Supervised/neural networks	Separation between HFOs and baseline activity
Blanco et al. 2010 [17]	Power ratio Spectral centroid Line length	Unsupervised/k-medoids	Separation between HFOs (Rs, FRs, Rs+ FRs) and artifacts
Dümpelmann et al. 2012 [18]	Short time energy Short time line length Short time instantaneous frequency	Supervised/RBF neural network	Discrimination between true and false HFOs
Matsumoto et al. 2013 [19]	Spectral amplitude Frequency Duration	Supervised/SVM	Discrimination between physiological and pathological HFOs
Chaibi et al. 2014 [20]	Mean/STD Teager energy Zero crossing Power Spectral density	Supervised/decision trees	Discrimination between HFOs and background activity
Liu et al. 2016 [21]	Spectral entropy Sub-band power ratio	Unsupervised/GMM	HFOs clustering
Ting et al. 2016 [23]	Fuzzy entropy Short time energy	Supervised/Fuzzy Neural networks	Distinction among HFOs and normal activity
Jrad et al. 2017 [9]	Energy ratio Duration	Supervised/SVM	Multi-classification of HFOs
Yuxiao et al. 2019 [24]	Teager energy Wavelet entropy	Semi-supervised/mean shift and k-means	HFOs clustering
Lachner-Piza et al. 2019 [25]	Amplitude variance Mean Teager energy Mean power	Supervised/SVM	Multi-classification of HFOs into 4 classes named: Rs, FRs, IESs co-occurring during Rs and IESs co-occurring during FRs
Sciaraffa et al. 2020 [26]	Root mean square energy Line length energy Short time energy Teager energy	Supervised/SVM; LDA; logistic regression; KNN	Multi-classification of HFOs into 3 classes named: Rs, FRs and FRs co-occurring during Rs

[7], [8] and High-Gamma (Hγ, [80-120 Hz]) [7], [8] bands. Thus, HFOs can be divided into four bands: γ ([30-80 Hz]), Hγ ([80-120 Hz]), Rs ([120-250 Hz]) and FRs ([250-500 Hz]). HFOs detection is traditionally performed by experts through a visual inspection from long hours of iEEG recordings [2]. However, such marking remains time-consuming and subjective [6]. To cope with this issue, several approaches [9], [10], [11], [12], [13], [14], [15] have been proposed in the literature aiming at providing automatic identification of these particular cerebral activities, and especially their discrimination from other transient events like Interictal Epileptic Spikes (IESs). Commonly, the HFOs detection procedures are split into detection and classification [9], [10], [11], [12], [13], [15] to cite a few, but, in the present study only the classification stage is considered. Therefore, existing approaches on detection and estimation of HFOs are out of the scope of this paper. A recent study [15] showed that HFOs

Accepted manuscript / Final version

and IESs are complementary biomarkers of the EZ. Hence, identifying relevant features for those biomarkers is a real need. The present study focuses on the prominent features for a multi-classification task with the aim of discriminating among the different HFOs and IESs. Until now, various algorithms have been developed for the classification of HFOs events. The principle of these algorithms involves machine learning approaches to extract relevant features and use them for HFOs classification. In this context, supervised and unsupervised machine learning algorithms (see Table 1) have been widely used. Firpi et al. [16] proposed an algorithm based on particle swarm optimization and neural networks to generate relevant features that separate HFOs and a baseline activity. An unsupervised cluster has been provided by Blanco et al. [17] to discriminate between HFOs and artifacts based on a k-medoids approach and some features in the time and frequency domains. To distinguish between true and false HFOs, Dümpelmann et al. [18] employed time features and radial basis function neural networks. Moreover, for a binary classification between physiological and pathological HFOs, Matsumoto et al. [19] employed a cascade of time and frequency features as an input to a Support Vector Machine (SVM) classifier. Chaibi et al. [20] associated several features with decision trees classifier to distinguish HFOs and background activity. To increase the discrimination among HFOs events and noise, Liu et al. [21] provided a Gaussian Mixture Model (GMM) based clustering. Approximate entropy [22] and fuzzy entropy [23] were also used to separate HFOs from normal activity. In the context of multi-classification of the HFOs events, Jrad et al. [9] considered energy ratio between bands and time duration as features. Recently, wavelet entropy and Teager energy were used in [24] for HFOs clustering using k-means and mean shift algorithms. More recently, other studies focused on the discrimination between different HFOs bands using root mean square energy [25], line length energy [25], [26], short time energy [26] and Teager energy [25] as features. for a complete review of conventional time, frequency and energy-based features, the reader can refer to [27].

As listed in Table 1, it is clear that the most frequent features in the literature come either from the time domain or from the frequency domain. However, a main drawback of those domains is the difficulty in providing any information about frequency variations over time. Hence, since HFOs are non-stationary, it is essential to describe their spectral change in time. Thus, the time frequency (TF) representation presents the advantage of merging both time and frequency information. Moreover, the TF representation has shown to be efficient in a number of neuroscience applications, for instance Alzheimer's disease identification [28], sleep stage classification [29], [30], or epileptic seizure classification [31], [32]. Recently, several studies have addressed the relevance of the TF representation in the context of HFOs classification [9], [21]. More particularly, Migliorelli et al. [33] proposed a set of relevant TF-based features for a binary classification of HFOs (i.e., HFOs vs no HFOs). However, no study has addressed the shape of HFOs events in the TF plane as a way to characterize them. Such shape related features can further be relevant for a complete description of HFOs events. Therefore, the novelty of the present contribution resides in combining TF and image related features derived from TF representations of HFOs as an adequate mean towards a complete characterization of HFOs and hence a more robust HFOs multiclassification task. To achieve high classification performances, extracting relevant TF features requires powerful TF representation tool. Most TF representations are based on short time Fourier transform (STFT), wavelet analysis such as the continuous wavelet transform (CWT) or Wigner Ville distribution (WVD). The major drawback of these TF representations is the cross-term which may cause noise in TF signal analysis. Hence, the Stockwell transform (S-transform) [34] has been developed to overcome the limits of the conventional representations. Thanks to its TF resolution, the S-transform provides a better visualization. This advantage makes this representation an appropriate tool in our study.

Accepted manuscript / Final version

In this paper, we propose a new approach to discriminate between five classes, namely γ, Hγ, Rs, FRs and IESs. More precisely, we proposed to firstly extract diverse features from a TF based S-transform representation [34] with the aim of tracking the energy distribution of the different five classes. Likewise, relevant image-based features derived from image processing tools such as image binarization and image gradient, commonly used in computer vision, are also used in this study to characterize the events of interest. Finally, the constructed feature vector, including both TF and image-related features, is provided as an input to a multi-class SVM classifier.

The remainder of the paper is organized as follows: Section II is dedicated to methodology. Numerical experiments are presented in Section III, discussion is given in Section IV and finally the conclusion in Section V.

II. METHODOLOGY

The present work proposes a new approach for the classification of γ, Hγ, Rs, FRs (i.e., HFOs) and IESs activities. It relies mainly on employing relevant features extracted, for each event of interest, from the corresponding TF representation and its associated TF grayscale image. These characteristics are then used to learn the classifier. A flow chart describing the main steps of the proposed approach is given in Fig. 1. More details regarding each step are presented in the subsequent subsections.

II.1. *Notations*

In the sequel, matrices are denoted by italic boldface capital letters, e.g., $\boldsymbol{A}$, vectors are denoted by italic boldface lowercase letters, e.g., $\boldsymbol{a}$, and scalars are denoted by italic lowercase letters, e.g., a. In addition, the $(i,j)th$ entry of a matrix $\boldsymbol{A}$ is denoted by $A(i,j)$. Besides, $|.|$ will denote either the absolute value function of real numbers or the magnitude in case of complex argument. In addition, $\top$ and $*$ stand for the transposition and the convolution operators, respectively.

II.2. *Data preprocessing*

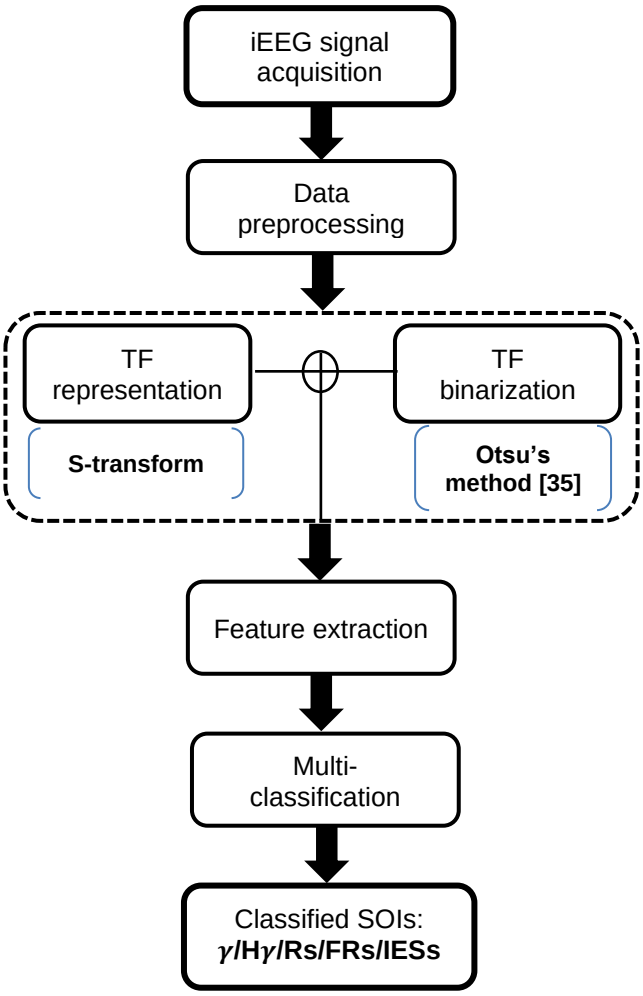


Fig. 1. Flowchart of the proposed HFOs classification method.

As the labeled segments of interest (SOIs) in our dataset are not of equal duration, the data preprocessing step consists in reframing each SOI into a $200\ \mathrm{ms}$ length one. This time period (i.e., $200\ \mathrm{ms}$) corresponds to the average of all periods of labeled events in our dataset. Then, each $200\ \mathrm{ms}$ -length SOI was first centered around $0\ \mathrm{ms}$ such that each event lasted from $-100\ \mathrm{ms}$ to $+100\ \mathrm{ms}$. Besides, in order to assess the relevance of the chosen time period of each SOI (i.e., $200\ \mathrm{ms}$), the performance of the proposed approach was also evaluated using different time periods ($60\ \mathrm{ms}$ and $600\ \mathrm{ms}$). The time period of $60\ \mathrm{ms}$ corresponds to the one of the shortest labelled SOI in our data set while the time period of $600\ \mathrm{ms}$ is the one of the largest labelled SOI. Numerical simulations have shown a highest performance of the proposed approach when a time period of $200\ \mathrm{ms}$ was

Accepted manuscript / Final version

used. An extensive description of this comparative study is provided as supplementary materials. Finally, in order to avoid the edge effect in each segment during the S-transform step, the obtained SOI was multiplied with a Hanning window of $200\ \mathrm{ms}$ length.

II.3. *Time-Frequency representation*

Once the SOIs have all the same duration, a TF representation of each SOI is then performed using the S-transform [34]. Let $x[n], n = 0,1,2,\cdots,N-1$ denotes a discrete time series corresponding to a given continuous time signal, where N denotes the number of time samples. Then, the S-transform of $x[n]$ computed at a given time shift factor $k \in \{0,\cdots,N-1\}$ and a frequency bin $m \in \{0,\cdots,M-1\}$, where M stands for the number of frequency bins, is defined as follows:

$$S[k,m] = \sum_{n=0}^{N-1} x[n]\,\omega[k-n,m]\,e^{-i2\pi\frac{m}{M}k} \qquad (1)$$

where $\omega[n,m]$ is a specific mother wavelet function given by:

$$\omega[n,m] = \frac{|m|}{M\sqrt{2\pi}} e^{-\frac{n^2m^2}{2M^2}} \qquad (2)$$

II.4. *Feature extraction*

In this step which is the core of the proposed approach, features are extracted not only from conventional raw TF representation [36] of each SOI but also from its associated TF grayscale image. Such transformed representation permits to employ specific features in the field of image analysis and processing as described below. For the sake of convenience, we note from now on $\bar{S}[k,m] = |S[k,m]|^2$.

II.4.1. *Raw Time-frequency features*

- Time-frequency flux (TF_{flux}) : a measure of the variation of the signal energy in the TF plane. It is defined by:

$$TF_{flux}[l,r] = \sum_{n=0}^{N-1-l}\sum_{m=0}^{M-1-r} \left|\bar{S}[n+l,m+r] - \bar{S}[n,m]\right| \qquad (3)$$

where l and r are the direction of the signal energy through the time and frequency axes, respectively. Three possible directions are considered in this study:
(i) along the time axis (i.e., $l=1$, $r=0$), noted $TF_{flux1} = TF_{flux}[1,0]$, (ii) along the frequency axis (i.e., $l=0$, $r=1$), noted $TF_{flux2} = TF_{flux}[0,1]$ and (iii) along both time and frequency axes (i.e., $l=r=1$), noted $TF_{flux3} = TF_{flux}[1,1]$.

- Time-frequency flatness ($TF_{flatness}$) : a measure to quantify the flatness of the distribution of the signal energy:

$$TF_{flatness} = \frac{\prod_{n=0}^{N-1}\prod_{m=0}^{M-1}\bar{S}[n,m]^{\frac{1}{MN}}}{\frac{1}{MN}\sum_{n=0}^{N-1}\sum_{m=0}^{M-1}\bar{S}[n,m]} \qquad (4)$$

- Energy concentration (EC) : a measure to quantify the concentration of the signal energy in the TF plane:

$$EC = \left(\sum_{n=0}^{N-1}\sum_{m=0}^{M-1}\bar{S}[n,m]^{1/2}\right)^2 \qquad (5)$$

- Statistical features: statistical features such as the mean (μ), standard deviation (σ), skewness (sk), kurtosis (ku) and the coefficient of variation (cv), are also considered. Conventionally, those features are employed separately either in the time or in the frequency domain. Recently, they have been extended to the TF domain and defined as follows [36]:

$$\mu = \frac{1}{MN}\sum_{n=1}^{N}\sum_{m=1}^{M}\bar{S}[n,m] \qquad (6)$$

$$\sigma = \sqrt{\frac{1}{MN}\sum_{n=1}^{N}\sum_{m=1}^{M}\left(\bar{S}[n,m]-\mu\right)^2} \qquad (7)$$

$$sk = \frac{1}{MN\sigma^3}\sum_{n=1}^{N}\sum_{m=1}^{M}\left(\bar{S}[n,m]-\mu\right)^3 \qquad (8)$$

$$ku = \frac{1}{MN\sigma^4}\sum_{n=1}^{N}\sum_{m=1}^{M}\left(\bar{S}[n,m]-\mu\right)^4 \qquad (9)$$

Accepted manuscript / Final version

$$cv = \frac{\sigma}{\mu} \quad (10)$$

II.4.2. *Time-frequency image feature*

In addition to the above TF features, other image-related ones are also employed. To this end, two transformations of the initial TF plane are performed: (i) binarization and (ii) binarization followed by an image gradient computation [37]. Image related features are then extracted from these two representations.

II.4.2.1. *Binary image features*

The TF representation of each SOI is transformed into a 8-bit grayscale image. Then, the obtained grayscale image is binarized using Otsu's method [35]. This method is widely used in image processing for image segmentation or binarization. For each obtained binary image, denoted here by Υ, geometric features are extracted. These features can be calculated using the image moment, $M_{p,q}$, of order $(p,q) \in \mathbb{N} \times \mathbb{N}$ defined as follows:

$$M_{p,q} = \sum_{n=0}^{N-1} \sum_{m=0}^{M-1} n^p m^q \Upsilon(n,m) \quad (11)$$

The moment based geometric features considered in our study are:

- The area: the number of pixels constituting the SOI in the image

$$\text{Area} = M_{0,0}$$

- The perimeter: the number of image pixels constituting the SOI boundary

$$\text{Perimeter} = \left(\left(M_{3,0} + M_{1,2} \right)^2 + \left(M_{0,3} + M_{2,1} \right)^2 \right)$$

- The compactness: a measure reflecting the SOI shape in the considered plane

$$\text{Compactness} = \frac{\text{Perimeter}^2}{\text{Area}}$$

- The centroid: the pixel at the center of the SOI shape with TF coordinates given by $\left(\frac{M_{1,0}}{M_{0,0}}; \frac{M_{0,1}}{M_{0,0}} \right)$.

II.4.2.2. *Image gradient features*

For each considered SOI, the gradient of its binarized TF representation is computed by convolving its associated binary image Υ with the gradient operator $\boldsymbol{h} = [-1\ 0\ 1]$. This convolution is performed through the time and frequency directions separately:

$$\boldsymbol{G}_t = \Upsilon * \boldsymbol{h} \quad (12)$$

$$\boldsymbol{G}_f = \Upsilon * \boldsymbol{h}^\top \quad (13)$$

where $\boldsymbol{G}_t$ and $\boldsymbol{G}_f$ are respectively the image gradients following the time and frequency axes. Then, the magnitude of the obtained gradient image [37], Γ, is computed as follows:

$$\Gamma = \sqrt{\boldsymbol{G}_t^{\,2} + \boldsymbol{G}_f^{\,2}} \quad (14)$$

Once the gradient image is computed, its $L1$-norm can be considered as a feature quantifying the sparsity of the resulting contour. This $L1$-norm is computed as follows:

$$\left\| \Gamma \right\|_1 = \sum_{n=0}^{N-1} \sum_{m=0}^{M-1} \left| \Gamma(n,m) \right| \quad (15)$$

A summary list of the TF extracted features is given in Table 2.

II.5. *Multi-class SVM classification*

Once the aforementioned features are computed, they are used to learn the classifier. In this study, the SVM algorithm is used for the multi-classification of the different events in our dataset. The choice of this algorithm comes from its efficiency which has been reported earlier in several EEG based multi-classification studies [9], [25], [26]. In this work, the radial basis function (RBF) widely used in the context of multi-classification problems is employed as a kernel for the SVM algorithm [38]. The RBF

Accepted manuscript / Final version

Table 2. List of extracted TF and image-related features.

Type	Name	Formula	Specificity
Raw TF feature	TF flux	$TF_{flux}[l,r]=\sum_{n=0}^{N-1-l}\sum_{m=0}^{M-1-r}\left\|\bar{S}[n+l,m+r]-\bar{S}[n,m]\right\|$	A measure of the variation of the signal energy in the TF plane
	TF flatness	$TF_{flatness}=\frac{\prod_{n=0}^{N-1}\prod_{m=0}^{M-1}\bar{S}[n,m]^{\frac{1}{MN}}}{\frac{1}{MN}\sum_{n=0}^{N-1}\sum_{m=0}^{M-1}\bar{S}[n,m]}$	A measure to quantify the flatness of the distribution of the signal energy
	Energy concentration	$EC=\left(\sum_{n=0}^{N-1}\sum_{m=0}^{M-1}\bar{S}[n,m]^{1/2}\right)^2$	A measure to quantify the concentration of the signal energy in the TF plane
	Mean	$\mu=\frac{1}{MN}\sum_{n=1}^{N}\sum_{m=1}^{M}\bar{S}[n,m]$	Statistical features
	Standard deviation	$\sigma=\sqrt{\frac{1}{MN}\sum_{n=1}^{N}\sum_{m=1}^{M}\left(\bar{S}[n,m]-\mu\right)^2}$	
	Skewness	$sk=\frac{1}{MN\sigma^3}\sum_{n=1}^{N}\sum_{m=1}^{M}\left(\bar{S}[n,m]-\mu\right)^3$	
	Kurtosis	$ku=\frac{1}{MN\sigma^4}\sum_{n=1}^{N}\sum_{m=1}^{M}\left(\bar{S}[n,m]-\mu\right)^4$	
	Coefficient of variation	$cv=\frac{\sigma}{\mu}$	
TF image feature	Area	$\text{Area}=M_{0,0}$	The number of pixels constituting the SOI in the image
	Perimeter	$\text{Perimeter}=\left(\left(M_{3,0}+M_{1,2}\right)^2+\left(M_{0,3}+M_{2,1}\right)^2\right)$	The number of image pixels constituting the SOI boundary
	Compactness	$\text{Compactness}=\frac{\text{Perimeter}^2}{\text{Area}}$	A measure reflecting the SOI shape in the TF plane
	Centroid	$\left(\frac{M_{1,0}}{M_{0,0}};\frac{M_{0,1}}{M_{0,0}}\right)$	The pixel at the center of the SOI shape with TF coordinates
	L1-norm	$\left\|\Gamma\right\|_1=\sum_{n=0}^{N-1}\sum_{m=0}^{M-1}\left\|\Gamma(n,m)\right\|$	A measure quantifying the sparsity of the image gradient contour

function is defined as $exp\left(-\beta\left\|\delta-\nu\right\|_2^2\right)$ where the variables δ and ν are two training samples and β denotes the width of the RBF function. Another important parameter to be taken into account for the SVM algorithm is the regularization parameter C, which is used to balance the relative importance of minimizing the training error and maximizing the margins between classes. To minimize the risk of model overfitting, the abovementioned parameters are wisely defined using the grid search method [39]. Besides, the widely used One-Against-All (OAA) technique [39] is employed to adapt the SVM algorithm, initially proposed for binary classification, to multi-classification tasks.

Accepted manuscript / Final version

III. NUMERICAL EXPERIMENTS

III.1. *iEEG dataset*

Both simulated and real iEEG signals are used in this study. More details regarding the description of these signals can be found in [9].

Briefly, the real iEEG signals were recorded in the Neurology Department of the University Hospital of Rennes, France from five patients who suffered from refractory epilepsy. All patients gave informed consent for participation in research studies. A 256-Brain Quick (Micromed, Italy) recording system with a sampling rate of 2048 Hz was used for data acquisition. The visual marking of HFOs events was done by two reviewers independently in LTSI, University of Rennes 1. A total number of 5174 marked events were employed in the present study. In fact, five classes γ, Hγ, Rs, FRs and IESs are taken into consideration in the annotation procedure and labeled as γ (1015), Hγ (1032), Rs (1053), FRs (1071), and IESs (1003).

To assess the performance of the proposed classification system, a study on simulated signals was also conducted. These signals were generated by adding simulated cerebral background activity to the real annotated events described above. The background activity was simulated by means of a computational model of neural population where sigmoid weights were used to control the background activity level. A signal to noise ratio (SNR) was defined to control the ratio between the event of interest and the background activity. This permits to evaluate the robustness of the proposed approach to several SNR values (-10, -5, 0, 5, 10 and 15 dB).

III.2. *Performance measures*

Several performance criteria are used in this study to evaluate the classification performance of the proposed approach. These criteria are the sensitivity (SEN), the specificity (SPE), the accuracy (ACC) and F1-score defined respectively as follows:

$$SEN = \frac{TP}{(TP + FN)} \tag{16}$$

$$SPE = \frac{TN}{(TN + FP)} \tag{17}$$

$$ACC = \frac{TP + TN}{(TP + TN + FN + FP)} \tag{18}$$

$$F1 - score = \frac{2TP}{2TP + FP + TN} \tag{19}$$

where TP, TN, FN, FP stand, respectively, the number of true positives, true negatives, false negatives and false positives.

Moreover, the SEN and SPE metrics are used to design a receiver operating characteristic (ROC) curve, from which the area under the ROC curve (AUC) is computed as a measure to assess the relevance of the SVM classifier.

All experiments and simulations in the present study were performed using MATLAB (Mathworks Inc., Natick, MA) for iEEG database processing and Python software for classification through the scikit-learn library (https://scikit-learn.org). Different simulations were run on an Intel(R) Xeon (R), 2.7 GHz (2 processors) with 32 Go memory.

III.3. *Feature extraction and analysis*

As mentioned previously (Section II.5), for each SOI, both TF and image-based features are used to learn the classifier. Fig. 2 shows for each SOI in our dataset (first row) (i) the TF plane (second row), (ii) the TF plane in a grayscale image form (third row), (iii) the binarized version of the TF grayscale image (fourth row) and (iv) the gradient representation of the TF grayscale image (fifth row). Each representation has its own specificity to characterize the considered SOI. For example, while the TF representation provides information regarding the energy distribution over the time and frequency domains, which can be revealed by adequate TF features such as TF_{flux} and $TF_{flatness}$, the image gradient based TF representation helps in shedding light upon the event contour which can be quantified using the $L1$ -norm. Features described previously are extracted for each SOI in our dataset. Then, in order to analyze the relevance of the selected features, a feature analysis based on violin plot representation [40] is adopted as depicted in Fig. 3. Such representation

Accepted manuscript / Final version

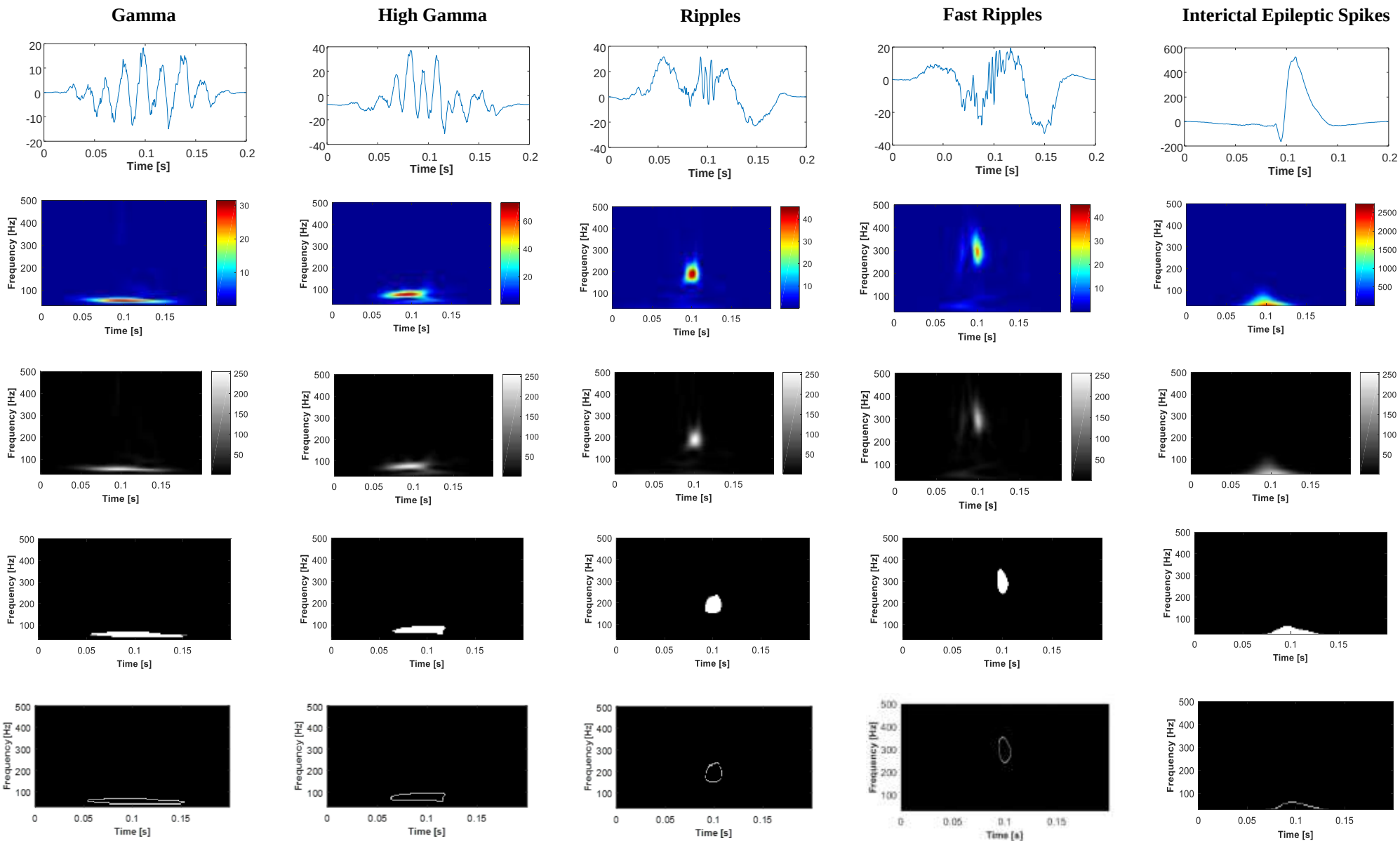


Fig. 2. Representation of HFOs and IESs patterns in time domain (first row) (i) TF plane (second row), (ii) TF based grayscale image (third row), (iii) binarized TF based grayscale image (fourth row) and (iv) TF based grayscale image gradient (fifth row).

Accepted manuscript / Final version

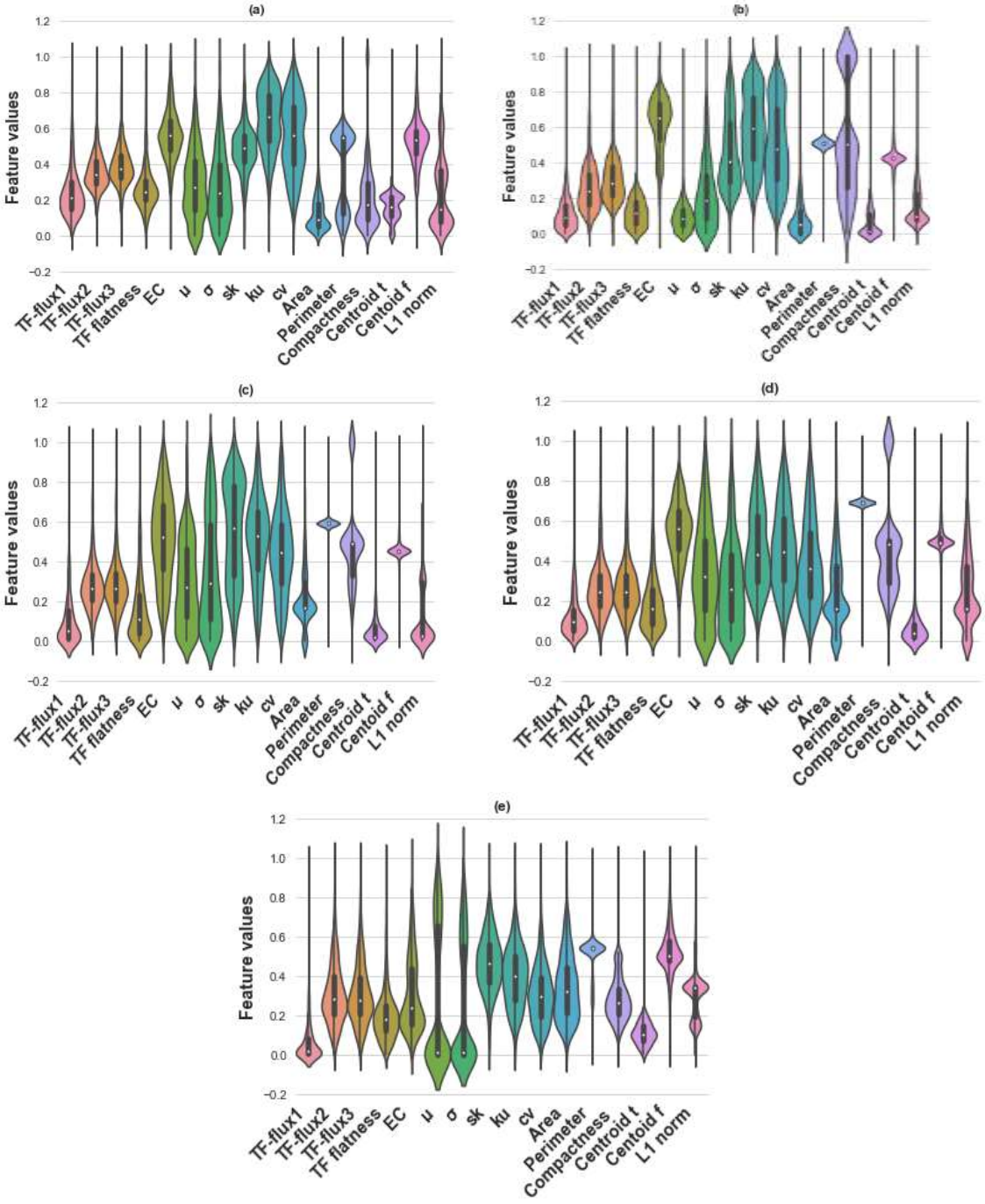


Fig. 3. Violin plots of the considered features of the five classes: (a): γ, (b): Hγ, (c): Rs, (d): FRs and (e): IESs.

combines statistical information that can be given by a simple boxplot representation with the distribution of the considered feature over the entire dataset. Furthermore, for the sake of comparability between all violin representations, a min-max normalization approach is applied to all computed features. Fig. 3 shows generally that, for each event (i.e., γ, Hγ, Rs, FRs and IESs), the selected features are discriminant since their corresponding violin plots are different in terms of both statistical information (median and quartiles) and feature distribution. Besides, even for those features with quasi-similar feature distributions (i.e., case of features *ku* and *cv*), their corresponding expected to provide a good classification of the segments of interest.

Accepted manuscript / Final version

Table 3. Classification performance of the proposed approach using simulated data, the mean (STD) of SEN, SPE, ACC, AUC and F1-score are reported.

SNR (dB)	SOI class	SEN	SPE	ACC	AUC	F1-score
+15	γ	0.999 (0.003)	0.999 (0.002)	0.999 (0.001)	0.997 (0.004)	0.998 (0.005)
	Hγ	0.987 (0.002)	0.996 (0.005)	0.995 (0.006)	0.990 (0.004)	0.987 (0.001)
	Rs	0.981 (0.002)	0.994 (0.006)	0.991 (0.007)	0.990(0.001)	0.982 (0.001)
	FRs	0.985 (0.002)	0.995 (0.006)	0.993 (0.007)	0.991 (0.003)	0.985 (0.001)
	IESs	1.000 (0.000)	1.000 (0.000)	1.000 (0.000)	1 (0.000)	1.000 (0.000)
	Average	**0.990 (0.001)**	**0.996 (0.003)**	**0.995 (0.004)**	**0.993 (0.002)**	**0.990 (0.001)**
+10	γ	1.000 (0.000)	0.999 (0.000)	0.999 (0.000)	0.999 (0.000)	0.999 (0.001)
	Hγ	0.987 (0.002)	0.997 (0.004)	0.995 (0.000)	0.990 (0.004)	0.989 (0.001)
	Rs	0.987 (0.001)	0.994 (0.000)	0.992 (0.000)	0.992 (0.001)	0.983 (0.001)
	FRs	0.986 (0.002)	0.997 (0.006)	0.994 (0.006)	0.992 (0.006)	0.988 (0.001)
	IESs	0.999 (0.003)	0.999 (0.001)	0.999 (0.001)	0.989 (0.001)	0.999 (0.003)
	Average	**0.991 (0.001)**	**0.997 (0.002)**	**0.995 (0.001)**	**0.992 (0.002)**	**0.991 (0.001)**
+5	γ	0.999 (0.001)	0.998 (0.000)	0.998 (0.000)	0.999 (0.004)	0.996 (0.001)
	Hγ	0.973 (0.005)	0.995 (0.001)	0.986 (0.001)	0.991 (0.001)	0.977 (0.004)
	Rs	0.976 (0.005)	0.989 (0.001)	0.993 (0.006)	0.993 (0.007)	0.971 (0.003)
	FRs	0.980 (0.004)	0.994 (0.001)	0.988 (0.001)	0.995 (0.001)	0.975 (0.003)
	IESs	0.998 (0.001)	0.999 (0.000)	0.999 (0.000)	0.999 (0.000)	0.998 (0.001)
	Average	**0.985 (0.003)**	**0.995 (0.000)**	**0.992 (0.001)**	**0.995 (0.002)**	**0.983 (0.002)**
0	γ	0.998 (0.001)	0.999 (0.000)	0.998 (0.000)	0.990 (0.007)	0.996 (0.001)
	Hγ	0.976 (0.005)	0.995 (0.001)	0.991 (0.001)	0.978 (0.001)	0.979 (0.003)
	Rs	0.973 (0.004)	0.991 (0.001)	0.987 (0.007)	0.998 (0.006)	0.972 (0.003)
	FRs	0.976 (0.004)	0.992 (0.001)	0.988 (0.001)	0.990 (0.002)	0.976 (0.003)
	IESs	0.999 (0.001)	0.999 (0.000)	0.999 (0.000)	0.999 (0.001)	0.998 (0.003)
	Average	**0.984 (0.003)**	**0.995 (0.000)**	**0.992 (0.001)**	**0.992 (0.003)**	**0.984 (0.002)**
-5	γ	0.998 (0.001)	0.998 (0.000)	0.998 (0.000)	1.000 (0.007)	0.996 (0.001)
	Hγ	0.967 (0.006)	0.993 (0.001)	0.994 (0.007)	0.994 (0.007)	0.980 (0.001)
	Rs	0.988 (0.001)	0.971 (0.004)	0.964 (0.006)	0.999 (0.006)	0.966 (0.004)
	FRs	0.974 (0.005)	0.990 (0.001)	0.986 (0.001)	0.995 (0.002)	0.972 (0.003)
	IESs	0.991 (0.001)	0.999 (0.000)	0.999 (0.000)	0.998 (0.001)	0.998 (0.001)
	Average	**0.983 (0.002)**	**0.990 (0.001)**	**0.988 (0.002)**	**0.997 (0.004)**	**0.982 (0.002)**
-10	γ	0.999 (0.005)	0.999 (0.001)	0.991 (0.001)	0.997 (0.004)	0.990 (0.004)
	Hγ	0.954 (0.002)	0.996 (0.005)	0.993 (0.006)	0.989 (0.001)	0.982 (0.001)
	Rs	0.980 (0.002)	0.961 (0.008)	0.961 (0.009)	0.992 (0.007)	0.967 (0.002)
	FRs	0.973 (0.002)	0.993 (0.007)	0.977 (0.008)	0.993 (0.001)	0.969 (0.001)
	IESs	0.988 (0.008)	0.991 (0.000)	0.994 (0.001)	0.999 (0.000)	0.992 (0.004)
	Average	**0.978 (0.003)**	**0.988 (0.004)**	**0.983 (0.005)**	**0.994 (0.002)**	**0.980 (0.002)**

Accepted manuscript / Final version

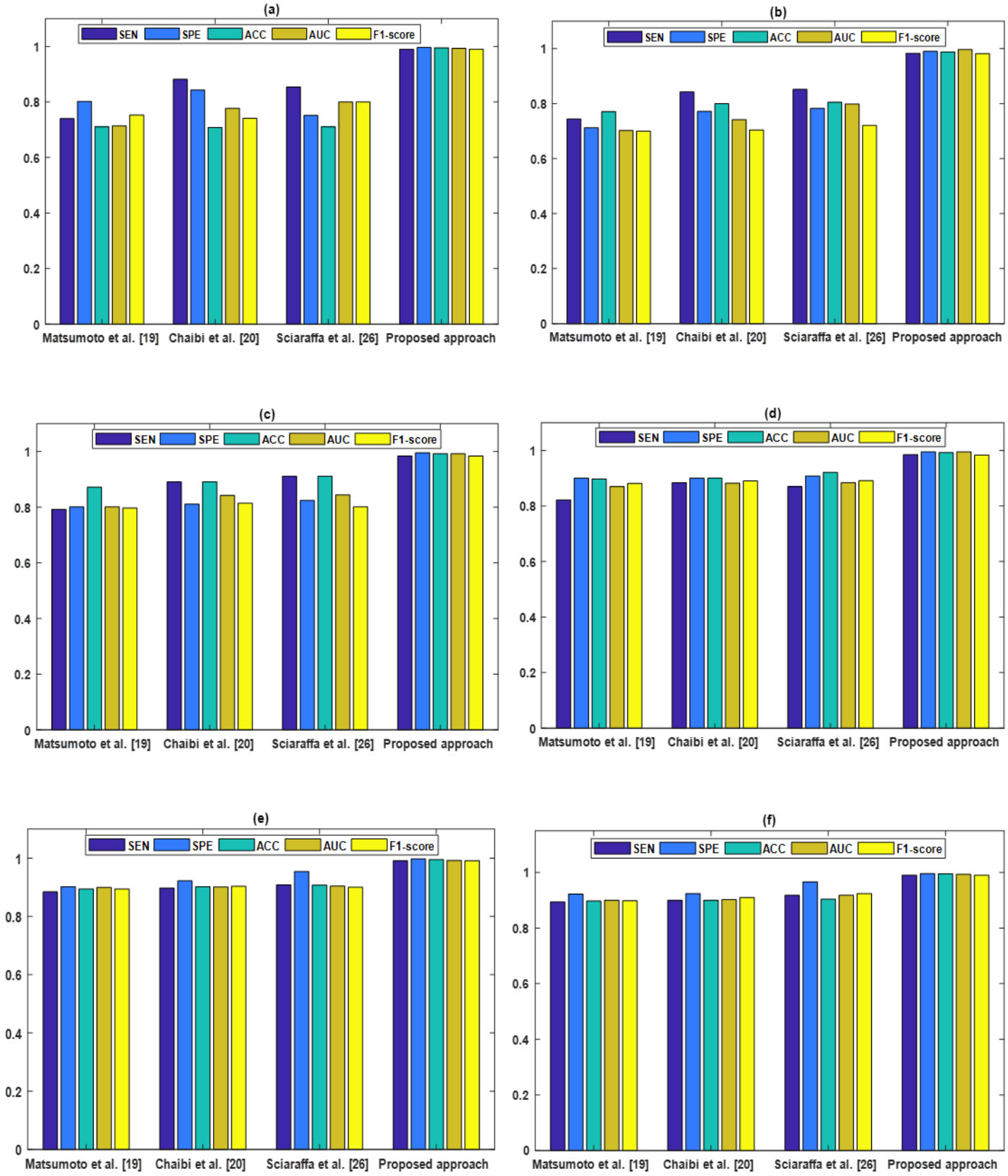


Fig. 4. Classification performance of the proposed approach compared to conventional ones using simulated data for different SNR values: (a): -10 dB, (b): -5 dB, (c): 0 dB, (d): 5 dB, (e): 10 dB and (f): 15 dB.

Accepted manuscript / Final version

III.4. *Events classification*

Once the features are computed, the next step consists in evaluating the performance of the proposed approach in classifying the five events γ, Hγ, Rs, FRs and IESs. This classification step is performed using the SVM classifier since the proposed approach has shown higher performance using such classifier compared to the other well-known *k*-nearest neighbor (KNN), naive Bayes (NB) and random forest (RF) ones. For a detailed description of this comparative study, the reader can refer to the provided supplementary materials. The performance evaluation study is conducted first using only simulated data and then using only real data. Here, each dataset (simulated and real data) is split into a training set (70%) and a test set (30%). Then, the training set is used to learn the optimal SVM-RBF hyperparameters C and β using the grid search method with a 5-fold cross validation scheme. Indeed, the retained couple (C, β), among a set of (C, β) candidates ((C, β) $\in \{1,10,100,1000,100000\} \times \{10^{-5}, 10^{-4}, 0.01, 0.1, 1\}$) defined over the search grid, is the one for which the smallest model prediction error is obtained. Once the optimal hyperparameters are found, the test set is then used to evaluate the model performance in terms of sensitivity, specificity, accuracy, AUC and F1-score. The above steps are repeated over 100 trials where, at each trial, the training and test sets are randomly reshuffled. Regarding the couple (C, β) of hyperparameters, the optimal value was (10 ,1) for the simulated data and (1,0.1) for the real ones.

III.4.1. Case of simulated events

The behavior of the proposed classification approach is first evaluated on a simulated dataset generated as described in subsection III.1 for several SNRs (-10, -5, 0, 5, 10 and 15 dB) and then compared to conventional methods where only time, frequency [19], [20] or energy-based [26] features are used.

Obtained classification results in terms of SEN, SPE, ACC, AUC and F1-score criteria are given in Table 3 for the different SNR values. The mean and the standard deviation (STD) of the different computed performance metrics were provided for each class of the HFOs events. In addition, an averaged performance score for each metric was used as suggested in [41] and [42]. The goal of this latter score is to get an overview on the performance of the proposed method. According to Table 3, a good classification performance can be observed for the proposed approach for all classes and for all SNR values. More particularly, at first glance, we note that SEN, SPE, ACC, AUC and F1-score criteria show, for all event types and SNR values, averaged values around 0.970, 0.990, 0.990, 0.990 and 0.970, respectively.

From a SNR point of view, the proposed classification strategy shows slightly lower performance for lower SNR values (i.e., -5 and -10 dB) compared to the case of relatively high SNR values (10 and 15 dB). For instance, for SNR of 15 dB, values of 0.990 (0.001), 0.996 (0.003), 0.995 (0.004), 0.993 (0.002) and 0.990 (0.001), are obtained respectively, for SEN, SPE, ACC AUC and F1-score criteria. However, for SNR value of -10 dB, these criteria have values of 0.978 (0.003), 0.988 (0.004), 0.983 (0.005), 0.994 (0.002) and 0.980 (0.002), respectively. This is probably due the fact that, for low SNR, events of interest are drowned in the background activity or at least their amplitude is very comparable to the one of the background activity.

Regarding the comparison of the proposed approach with the abovementioned conventional methods [19], [20], [26], Fig. 4 shows the performance of the proposed approach in terms of SEN, SPE, ACC, AUC and F1-score for different SNR values i.e.,-10, -5, 0, 5, 10 and 15 dB. According to this figure, a higher classification performance of the proposed approach compared to the conventional methods can be noticed, especially for low SNR values. For instance, while the approach in [25] shows, for SNR equal to -10 dB, values of 0.854, 0.752, 0.711, 0.800 and 0.800 for SEN, SPE, ACC, AUC and F1-score, respectively, the proposed approach provides values of 0.978, 0.998, 0.983, 0.994 and 0.980 for the same criteria. Similarly, the proposed approach provides also higher classification scores compared to [19] and [20].

Accepted manuscript / Final version

III.4.2. *Case of real data*

The proposed approach has been also evaluated on real data in terms of SEN, SPE, ACC, AUC and F1-score. Hence, the mean and the STD of the different performance metrics are provided in Table 4 for each class of the HFOs events. According to this table, the proposed approach shows an averaged classification performance of 0.765 (0.025), 0.941 (0.006), 0.906 (0.006), 0.929 (0.005) and 0.768 (0.016), respectively. The relatively low value of the SEN criterion (0.765) compared to the one of the SPE (0.941) and ACC (0.906) is probably due to a lack of class separability in the trained classifier. However, despite the relatively low value of the SEN criterion, a high AUC value (0.929) is obtained. Furthermore, from event point of view, Table 4 shows that the best classification results are obtained for γ and FRs events with SEN value of 0.846 (0.025) and 0.825 (0.025), respectively.

Regarding the comparison of the proposed approach with conventional approaches [19], [20], [26], results in terms of SEN, SPE, ACC, AUC and F1-score are depicted in Fig. 5. According to this figure, we note again a higher classification performance for the proposed approach. For instance, while averaged values of 0.765, 0.941, 0.906, 0.929 and 0.768 of SEN, SPE, ACC AUC and F1-score criteria are respectively obtained for the proposed approach, lower values respectively equal to 0.529, 0.811, 0.852, 0.807, and 0.697 are obtained using the method proposed in [26]. Similarly, methods proposed in [19] and [20] show lower multiclassification performance compared to the proposed approach. In fact, the lowest behavior is noticed for the method developed in [19] as depicted in Fig. 5.

Table 4. Classification performance of the proposed approach using real data, the mean (STD) of SEN, SPE, ACC, AUC and F1-score are reported.

SOI class	SEN	SPE	ACC	AUC	F1-score
γ	0.846 (0.025)	0.963 (0.005)	0.940 (0.006)	0.970 (0.001)	0.848 (0.016)
Hγ	0.717 (0.025)	0.882 (0.010)	0.849 (0.008)	0.866 (0.006)	0.655 (0.017)
Rs	0.694 (0.024)	0.939 (0.007)	0.889 (0.007)	0.877 (0.012)	0.719 (0.018)
FRs	0.825 (0.025)	0.965 (0.005)	0.936 (0.006)	0.953 (0.004)	0.843 (0.015)
IESs	0.747 (0.026)	0.956 (0.005)	0.916 (0.006)	0.982 (0.006)	0.775 (0.017)
Average	**0.765 (0.025)**	**0.941 (0.006)**	**0.906 (0.006)**	**0.929 (0.005)**	**0.768 (0.016)**

Accepted manuscript / Final version

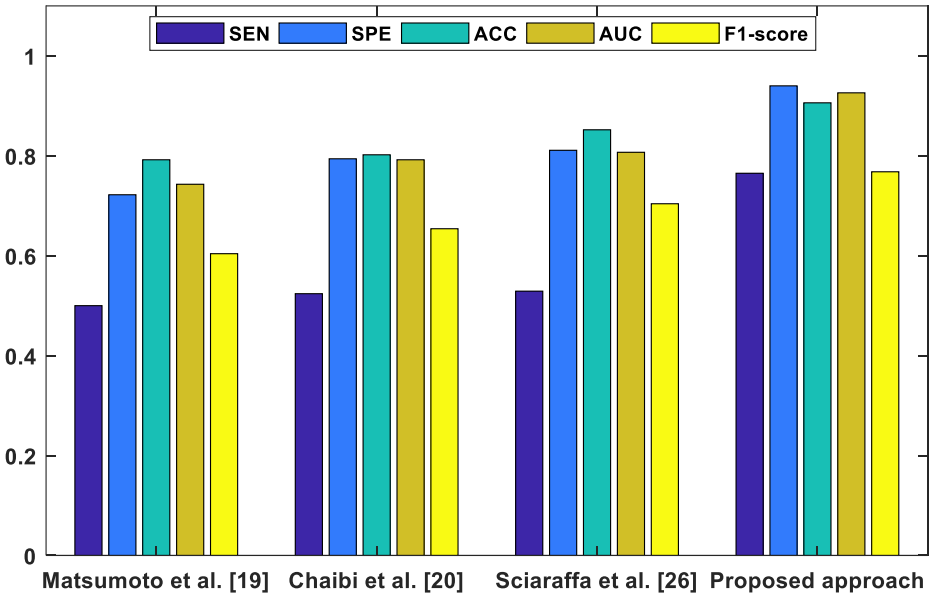


Fig 5. Classification performance of the proposed approach compared to conventional ones using real data.

IV. DISCUSSION

In this study a new approach for the classification of HFOs (γ, Hγ, Rs, FRs) and IESs activities was proposed. This approach relies mainly on employing relevant TF and image-based features to characterize the events of interest. These features allow for a complete characterization of these events in both time and frequency domains, simultaneously.

On the methodological level, thanks to its efficiency [33], [43], the S-transform was used to compute the TF representation of each SOI. This transform provides an efficient TF representation to reveal different TF and related image-based features. To the best of our knowledge, no study has yet addressed HFOs and IESs classification by employing simultaneously TF and image-based features. Such combination of TF and image-based features as proposed in this paper led to a very competitive classification performance in terms of SEN, SPE, ACC, AUC and F1-score, as shown in the previous section. More particularly, the proposed approach provides generally good performance results using simulated data as shown in Table 3, for all considered SNR values. However, a slight decrease in performance has been noticed in the case of low SNRs (i.e., -10 dB and -5 dB). Regarding the performance of the proposed approach on real iEEG recordings, a good behavior was still observed compared to the conventional approaches [19], [20] and [26] which is based only on time, frequency and energy features. Indeed, the proposed method achieved a good specificity across all HFOs classes with a good averaged value of 0.929 for the AUC criterion.

In fact, the good behavior of the proposed approach brings out the relevance of the employed TF and image-based features. This fact holds true for both simulated and real data.

The major finding in our work concerns the fact that TF features combined with image-based ones are a promising tool for multi-classification of HFOs and IESs. However, there are some limitations in the present study, which should be highlighted for future research. On the one hand, the proposed approach could suffer from the curse of dimensionality problem. This is mainly due to the dimensionality of the input feature vector which is proportional to the number of TF and image-based features. Such an issue can be dealt with by resorting to deep learning that allows for an automatic extraction of the most

Accepted manuscript / Final version

relevant TF and image-based features. In fact, deep learning has proved its relevance in image and signal processing areas. Even for HFOs classification, some studies such as [44], [45], to cite a few, have employed the CNN as a powerful deep learning tool. However, resorting to deep learning requires the data set to be large enough for a reliable network training step. Such condition is not fulfilled in the current study and stands, on the second hand, for an another limitation to be pointed out here. Therefore, future work would concern the collect of more clinical data for a more complete assessment.

V. Conclusion

The present paper investigated a new approach for HFOs classification method based on TF representation of events of interest. Several SOIs are projected in the TF domain using S-transform and from which several TF and image-based features were extracted. The efficiency of the proposed approach in terms of SEN, SPE, ACC, AUC and F1-score has been assessed through numerical experiments using simulated and real iEEG recordings. Obtained results support our claim that combining TF and image-based features are a promising tool to characterize events of interest in time and frequency domains, simultaneously and consequently to provide a powerful multi-classification of HFOs and IESs.

ACKNOWLEDGMENTS

The research reported in this paper was developed as a part of the PHC (Partenariat Hubert Curien) Project CREDIADIC n°41711PK, CMCU Code 19G1411.

DECLARATION OF COMPETING INTEREST

The authors declare that they have no known competing financial interests or personal relationships that could have appeared to influence the work reported in this paper.

REFERENCES

[1] Epilepsy – World Health Organization. Available from: http:// www.who.int/news-room/fact sheets/detail/epilepsy, 2019.

[2] J. Jacobs, R. J. Staba, E. Asano, H. Otsubo, J. Y. Wu, M. Zijlmans, I. Mohamed, P. Kahane, F. Dubeau, V. Navarro and J. Gotman, 'High frequency oscillations (HFOs) in clinical epilepsy', *Prog. Neurobiol.*, 98 (3): 302-315, 2012.

[3] A. Shoeibi, N. Ghassemi, M. Khodatars, M. Jafari, P. Moridian, R. Alizadehsani, A. Khadem, Y. Kong, A. Zare, J. M. Gorriz, J. Ramirez, M. Panahiazar, A. Khosravi and S. Nahavandi, 'Applications of epileptic seizures detection in neuroimaging modalities using deep learning techniques: methods, challenges, and future works', arXiv preprint arXiv: 2105.14278v1, 2021.

[4] A. Shoeibi, N. Ghassemi, R. Alizadehsani, M. Rouhani, H. Hosseini-Nejad, A. Khosravi, M. Panahiazar and S. Nahavandi, 'A comprehensive comparison of handcrafted features and convolutional autoencoders for epileptic seizures detection in EEG signals', Exp. Syst. Appl., 163:113788, 2021.

[5] A. Shoeibi, N. Ghassemi, M. Khodatars, P. Moridian, R. Alizadehsani, A. Zare, A. Khosravi, A. Subasi, U. R. Acharya and J. M Gorriz, 'Detection of epileptic seizures on EEG signals using ANFIS classifier, autoencoders and fuzzy entropies,' arXiv preprint arXiv: 2109.04364, 2021.

[6] M. Zijlmans, P. Jiruska, R. Zelmann, F. S. S. Leijten, J. G. R. Jefferys and J. Gotman, 'High-frequency oscillations as a new biomarker in epilepsy', *Ann. Neurol.* 71 (2): 169-178, 2012.

[7] P. J. Uhlhaas, G. Pipa, S. Neuenschwander, M. Wibral, and W. Singer, 'A new look at gamma? highlight- (>60 Hz) γ-band activity in

Accepted manuscript / Final version

cortical networks: Function, mechanisms and impairment', *Prog. in Biophy. And Mol. Biol*., 105(1-2): 14-28, 2011.

[8] S-C. Park, S. K. Lee, H. Che, and C. K. Chung, 'Ictal high-gamma oscillation (60–99Hz) in intracranial electroencephalography and postoperative seizure outcome in neocortical epilepsy', *Clin. Neuro*. 123(6):1100-1110, 2012.

[9] N. Jrad, A. Kachenoura, I. Merlet, F. Bartolomei, A. Nica, A. Biraben and F. Wendling, 'Automatic detection and classification of high frequency oscillations in depth-EEG signals', *IEEE Trans. Biomed. Eng*., 64(9): 2230–2240, 2016.

[10] G. Birot, A. Kachenoura, L. Albera, C. Bénar and F. Wendling, 'Automatic detection of fast ripples', *J. Neurosci. Methods*, 213(2):236-249, 2013.

[11] R. J. Staba, C. L. Wilson, A. Bragin, I. Fried and J. Engel Jr, 'Quantitative analysis of high-frequency oscillations (80–500 Hz) recorded in human epileptic hippocampus and entorhinal cortex', *J. of. Neuro*., 88(4): 1743-1752, 2002.

[12] A. B. Gardner, G. A. Worrell, E. Marsh, D. Dlugos and B. Litt, 'Human and automated detection of high-frequency oscillations in clinical intracranial EEG recordings', *Clin. Neuro*., 118(5): 1134-1143, 2007.

[13] B. Crépon, V. Navarro, D. Hasboun, S. Clemenceau, J. Martinerie, M. Baulac, C. Adam and M. Le Van Quyen, 'Mapping interictal oscillations greater than 200 Hz recorded with intracranial macroelectrodes in human epilepsy', *Brain*, 133(1):33-45, 2010.

[14] F. Krikid, S. Chaibi, A. Karfoul, A. Kachouri and R. Le Bouquin Jeannes, 'A comparative study between three epileptic high frequency oscillations detection strategies', *17th IEEE Int. Multi-conf. (S.S.D)*, 631-635, 2020.

[15] N. Roehri and F. Bartolomei, 'Are high-frequency oscillations better biomarkers of the epileptogenic zone than spikes?', *Curr. Opin. Neuro.*, 32(2):213-219, 2019.

[16] H. Firpi, O. Smart, G. Worrell, E. Marsh, D. Dlugos and B. Litt, 'High-frequency oscillations detected in epileptic networks using swarmed neural-network features', *Ann. Biomed. Eng.,* 35(9):1573–1584, 2007.

[17] J. A. Blanco, M. Stead, A. Krieger, J. Viventi, W R. Marsh, K. H. Lee, G. A. Worrell and B. Litt, 'Unsupervised classification of high-frequency oscillations in human neocortical epilepsy and control patients', *J. Neurophy.*, 104(5): 2900–2912, 2010.

[18] M. Dümpelmann, J. Jacobs, K. Kerber and A. Schulze-Bonhage, 'Automatic 80 – 250 Hz "ripple" high frequency oscillation detection in invasive subdural grid and strip recordings in epilepsy by a radial basis function neural network', *Clin. Neuro.*, 123(9): 1721–1731, 2012.

[19] A. Matsumoto, B. H. Brinkmann, S. Matthew Stead, J. Matsumoto, M.T Kucewicz, W. R. Marsh, F. Meyer and G. Worrell, 'Pathological and physiological high-frequency oscillations in focal human epilepsy', *J. Neuro.,* 110(8): 1958–1964, 2013.

[20] S. Chaibi, T. Lajnef, M. Samet, K. Jerbi and A. Kachouri, 'Detection of high frequency oscillations (HFOs) in the 80–500 Hz range in epilepsy recordings using decision tree analysis', *Int. Image Process. Appl. And Syst. Conf. IPAS*, 1-6, 2014.

[21] S. Liu, Z. Sha, A. Sencer, A. Aydoseli, N. Bebek, A. Abosch, T. Henry, C. Gurses and N. F. Ince. 'Exploring the time-frequency content of high frequency oscillations for automated identification of seizure onset zone in epilepsy', *J. Neural Eng*., vol. 13(2): 026026, 2016.

Accepted manuscript / Final version

[22] A. López-Cuevas, B. Castillo-Toledo, L. Medina-Ceja, C. Ventura-Mejía and K. Pardo-Peña, 'An algorithm for on-line detection of high frequency oscillations related to epilepsy', *Comp. Methods Programs Biomed*., 110(3): 354–360, 2013.

[23] W. Ting, M. Wu, X. Wan and Y. Du. 'Automatic detection of high frequency oscillations based on Fuzzy entropy and Fuzzy neural network', *35th Chinese Control Conference (CCC), Chengdu*, 5027-5032, 2016.

[24] D. Yuxiao, B. Sun, R. Lu, C. Zhang and H. Wu. 'A method for detecting high-frequency oscillations using semi-supervised *k*-means and mean shift clustering', *Neurocomputing*, 350:102–107, 2019.

[25] D. Lachner-Piza, J. Jacobs, J. C. Bruder, A. Schulze-Bonhage, T. Stieglitz and M. Dümpelmann. 'Automatic detection of high-frequency-oscillations and their sub-groups co-occurring with interictal-epileptic-spikes', *J. Neural. Eng*.,17(1):016030, 2020.

[26] N. Sciaraffa, MA. Klados, G. Borghini, G. Di Flumeri, F. Babiloni and P. Aricò, 'Double-step machine learning based procedure for HFOs detection and classification', *Brain*, 10(4): 220, 2020.

[27] C.J. Park, S.B. Hong. 'High frequency oscillations in epilepsy: Detection methods and considerations in clinical application', *J Epilepsy Res.,* 9:1-13, 2019.

[28] G. Fiscon, E. Weitschek, A. Cialini, G. Felici, P. Bertolazzi, S. De Salvo, A. Bramanti, P. Bramanti and M. C. de Cola. 'Combining EEG signal processing with supervised methods for Alzheimer's patients classification', *BMC Med. Info. and Decision Making*, 18, 35, 2018.

[29] P. Ghasemzadeh, H. Kalbkhani and M. G. Shayesteh, 'Sleep stages classification from eeg signal based on Stockwell transform', *IET Signal Process*, 13(2):242–252, 2018.

[30] O. Tsinalis, P. M. Matthews and Y. Guo, 'Automatic sleep stage scoring Using Time-Frequency Analysis and Stacked Sparse Autoencoders', *Ann. Biomed. Eng.,* 44(5):1587-1597, 2016.

[31] P. T. Krishnan, and P. Balasubramanian, 'Automated EEG seizure detection based on S-transform', *IEEE International Conference on Computational Intelligence and Computing Research (ICCIC), Chennai*, 1-5, 2016.

[32] A. Shoeibi, M. Khodatars, N. Ghassemi, M. Jafari, P Moridian, R. Alizadehsani, M. Panahiazar, F. Khozeimeh, A. Zare, H. Hosseini-Nejad, A. Khosravi; A.F. Atiya, D. Aminshahidi, S. Hussain, M. Rouhani; S. Nahavandi, U.R. Acharya, 'Epileptic seizures detection using deep learning techniques: a review', *Int. J. Environ. Res. Publ. Health*, 18: 5780, 2021.

[33] C. Migliorelli, A. Bachiller, J. F. Alonso, S. Romero, J. Aparicio, J. Jacobs-Le Van, M. A. Mananas and V. San Antonio-Arce, 'SGM: a novel time-frequency algorithm based on unsupervised learning improves high-frequency oscillation detection in epilepsy', *J Neural Eng*.17(2):26032, 2020.

[34] R.G. Stockwell, L. Mansinha and R. Lowe, 'Localization of the complex spectrum:the S transform', *IEEE Trans. Signal Process*, 44 (4):998–1001, 1996.

[35] N. Otsu, 'A threshold selection method from gray-level histograms', *IEEE Trans. Syst. Man. Cybern,* 9, 62–66, 1979.

[36] B. Boashash, G. Azemi and N. Ali Khan, 'Principles of time-frequency feature extraction for change detection in non-stationary signals: applications to newborn EEG abnormality

Accepted manuscript / Final version

detection', *Pattern Recognit*., 48, 616-627, 2015.

[37] J. Abudhamid Mohamed Saif, M. Hassan Hammad and I. A. A. Alqubati, 'Gradient Based Image Edge Detection', *IACSIT International Journal of Engineering and Technology*, 8 (3):153:156, 2016.

[38] K. Fu, J. Qu, Y. Chai and Yong Dong. 'Classification of seizure based on the time-frequency image of EEG signals using HHT and SVM', *Biomed. Signal Process. Control,*13:15-22, 2014.

[39] C-F. Chao and M.-H. Horng. 'The Construction of Support Vector Machine Classifier Using the Firefly algorithm'*, Comp. Intelli. And Neuro,* 2015:212719, 2015.

[40] M. Waskom, 'Seaborn: Statistical Data Visualization Seaborn', Accessed: Oct. 30, 2019. [Online]. Available: *http://seaborn.pydata.org.*

[41] A Alhudhaif, 'A novel multi-class imbalanced EEG signals classification based on the adaptive synthetic sampling (ADASYN) approach', *PeerJ Comput Sci*., 7: e523, 2021.

[42] P. Memar and F. Faradji, 'A Novel Multi-Class EEG-Based Sleep Stage Classification System'. *IEEE Transactions on Neural Systems and Rehab. Eng.*, 26(1), 84-95, 2018.

[43] S. Burnos, P. Hilfiker, O. Surcusu, F. Scholkmann, N. Krayenbuhl, T. Grunwald and J. Sarnthein, 'Human intracranial high frequency oscillations (HFOs) detected by automatic time-frequency analysis', *PLoS One*, 9(4): e94381, 2014.

[44] R. Zuo, J. Wei, X. Li, C. Li, C. Zhao, Z. Ren, Y. Liang, X. Geng, C. Jiang, X. Yang and X. Zhang, 'Automated detection of high-frequency oscillations in epilepsy based on a convolutional neural network', *Front. Comput. Neurosci.*, 13(6), 2019.

[45] B. Zhao, W. Hu, C. Zhang, X. Wang, Y. Wang, C. Liu, J. Mo, X. Yang, L. Sang, Y. Ma, X. Shao, K. Zhang and J. Zhang, 'Integrated automatic detection, classification and imaging of high frequency oscillations with stereoelectroencephalography', *Front. in Neurosci*., 14(546), 2020.

Accepted manuscript / Final version